ISIJ International, Vol. 54 (2014), No. 3, pp. 475–481

Evolution of Non-Metallic Inclusions in Ultra Low Carbon Steel after Aluminum Deoxidization

Myung-Duk SEO,[1)] Jung-Wook CHO,[2)]* Kwang-Chun KIM[3)] and Seon-Hyo KIM[1)]

1) Department of Materials Science and Engineering, Pohang University of Science and Technology (POSTECH), Pohang 790-784, Republic of Korea. 2) Graduate Institute of Ferrous Technology, Pohang University of Science and Technology (POSTECH), Pohang 790-784, Republic of Korea. 3) Steelmaking Technology Development Group, POSCO Gwangyang Works, Gwangyang 545-711, Republic of Korea.

(*Received on September 4, 2013; accepted on January 7, 2014*)

A new technique based on the PDF (Population Density Function) was suggested to investigate the behavior of non-metallic inclusions after deoxidization. In comparison with the traditional analysis using the size histogram of inclusions, the application of PDF can make it possible to attain more useful information to understand the evolution of inclusions such as the period of formation and mechanism for growth. In this study, the PDF of alumina inclusions was investigated for the ultra low carbon grade steel of 20 ppm C. The lollypop samples were taken at three stages after deoxidization using aluminum; at the end of RH degassing process, at tundish during casting operations, and in cast slabs after solidification. For all the samples except for the contaminated ones, the PDF shows a fractal distribution. The exponent in fractal distribution was –3.54 near the end of RH process at 7–13 minutes after deoxidization, which is similar with the previously reported value. In contrast, the exponent was changed to –2.76 in tundish and –2.38 in cast slab, respectively. Different expressions of the fractal distribution can be attributed to the changes in fluid condition of molten steel. The application of PDF also provides the quantitative evaluation for abnormal reoxidization of molten steel. The deviation of PDF from the reference distribution is in accordance with other evidences of reoxidization of molten steel such as the increase of nitrogen pick-up and the decrease of soluble aluminum.

KEY WORDS: non-metallic inclusion; steelmaking; population distribution function; reoxidization.

1. Introduction

Controlling non-metallic inclusions in steel is the most important key to improve both the quality and the productivity of steelmaking processes. In general, non-metallic inclusions are considered to be detrimental to the final steel product and also negatively affect the process by depositing in the feeding systems of continuous casting. Therefore, controlling the population of non-metallic inclusions in steel draws attention for its strong effects on the performance of refining process. Because the size distribution of the inclusion population after deoxidization is the result of the processes of nucleation, growth and removal, the interpretation of each size distribution can be used to provide valuable information on the growth and nucleation histories and growth mechanisms.

Considerable attention has been paid to the prediction of inclusion growth in molten steel over the past several decades.[1–7)] Zhang *et al.*[1)] studied the size distribution of Al_2O_3 inclusions after deoxidization of steel according to the static model by considering the theories of nucleation, growth by diffusion and the various mechanisms of collision. Kwon[4)] modified it into dynamic model in consideration of inclusion removal, time and space dependence of temperature and fluid patterns in ladle by a Computational Fluid Dynamics (CFD) model. It is known that the inclusion size distribution can change with time, from a lognormal distribution at the early stage after nucleation to a fractal distribution at a later state after growth.[1,4–7)] The previous studies[1,4,5)] showed that one or more of these growth processes dominate the overall growth of inclusions at various stages of the refining process. It is worthy to note that these size distribution follow the same tendency as a obtained data experimentally.[9–13)] The size distribution is initially narrow, with a maximum of the number density located at small size. With time, the size distribution become broader and is shifted to larger size.

According to Zhang *et al.*[1)] and Kwon,[4)] the inclusion size distribution is converted as density function according to the time and inclusion size. However, the density function obtained from their results should be variable depending on the bin size definition. To overcome this problem, Ende[6,8)] and Zinngrebe *et al.*[7)] applied PDF (Population Density Function) method into the analysis of inclusions evolution

This article is one which was originally scheduled for publication in the special issue (Vol. 54, No. 2) on "Cutting Edge of Computer Simulation of Solidification, Casting and Refining" and instead was specially published in this regular issue.

* Corresponding author: E-mail: Jungwook@postech.ac.kr

DOI: http://dx.doi.org/10.2355/isijinternational.54.475

in Ti-alloyed Al-killed steel. Because the application of PDF eliminates the arbitrariness caused by the different size of the bins, the PDF is believed to be useful to obtain a general expression for the size distribution of any inclusions in steel. This technique was originally developed in the chemical engineering industry by Randolf[14] and applied to geologic systems by Marsh[15,19] and Higgins.[16–18] Therefore, there have not been sufficient studies for the systematic comparison between the density function and PDF of inclusions in steel, in spite of potential metallurgical importance.

In this study, the PDF of alumina inclusions was investigated for the Ti-alloyed Al-killed ultra low carbon steels. After Al deoxidization, the evolution of alumina inclusion was analyzed at RH, T/D and Slab to quantify the PDF at various periods during steelmaking and casting. Also, the changes of PDF due to the abnormal operations have been evaluated especially when the molten steel is reoxidized. The obtained PDF results in this study were compared with numerical analysis results from previous numerical and experimental reports.[1,7]

2. Experimental

The lollypop samples were taken several times after aluminum deoxidization; at the end of RH degassing process, at tundish during casting operations, and in slabs.

To analyze the inclusions in the samples, an automated SEM technique was carried out. Also a stereological correction program has been applied using CSD Correction,[20] which convert 2D sectional data into 3D particle size distribution data.

2.1. Sampling

The secondary steelmaking and the casting processes for this study have been carried out as follows;

i. During RH degassing process, the molten steel was deoxidized by Al after decarburization, followed by Fe–Ti alloy addition 3 minutes later. Then Circulation of molten steel process was executed for 5–10 minutes.
ii. Transfer to the rotating turret of the caster.
iii. After opening the sliding gate of a 270 ton ladle, steel was cast into a two-strand 80 ton tundish.

The lollypop samples were taken at six stages; after deoxidization of molten steel, after Fe–Ti alloy addition during RH degassing, at the end of RH degassing process, at tundish when amount of molten steel in ladle corresponds to 150 ton and 50 ton, and in cast slabs after solidification. As shown in **Figs. 1** and **2**, the depth of submerged sampler at RH and Tundish is 500 mm. In total, 90 steel samples of 16 series were analyzed for this study.

2.2. Automated Inclusion Analysis (AIA) SEM Technique

Recently, an automated SEM technique has become available, which enables the comprehensive examination of the chemical and physical properties such as composition, morphology and size of inclusions. For the inclusion analysis, steel blocks which were applied to the spark-OES test were cut out from lollypop samples. The dimension of cut sample was 10 mm × 10 mm. Then, the blocks were mounted in resin and polished for inclusion analysis. To improve the reliability, the cross section for analysis was restricted to 8 mm × 8 mm (64.0×10^{-6} m^2). The AIA has been carried out using a Jeol JSM6980LV SEM at 20 kV and equipped with an EDS Oxford System. A feature sizing setup was as follows: 250× magnification, 0.247 um pixel size, and a 4×4 pixel minimum size corresponding to a lower limit of 0.75 um^2. Inclusions were detected on Back Scatter Electron mode image using automatic thresholding of the image grey level. Residual matrix spectra were quantified for Mg, Al, N, S, Ca, Ti, Fe, Mn, Cu, O. All object residual spectra and analysis results were recorded.

2.2.1. Correction of AIA Data

Generally the AIA data include many types of noisy information such as dust and hole. To eliminate them from data, Filtering routine was used, based on chemical compositions. After application of the filter, dust and scratch have to be removed. On average, more than 50% of all detected objects had to be removed as contaminations in the data. After data cleansing process, the largest inclusion data had 38 910 and the smallest had 190 individual inclusions from the sample of 8 × 8 mm.

2.3. Inclusion Population Density Function

Once the inclusion data has been processed to remove any artifacts, the 2D size distribution of the inclusions can be derived from the AIA measurements on the particle cross sectional area. The AIA data for polished blocks include physical and chemical information of inclusions such as length, area, width, shape and chemical composition. SEM inclusion analysis has a stereological limitation due to the 2 dimensional observations. In order to overcome this problem, The AIA data were transformed to the PDF size distribution using CSD Correction program[20] which was developed for conversion of 2D sectional data into 3D.

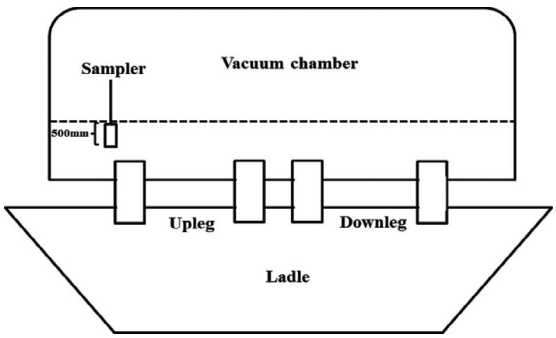

Fig. 1. Sampling position at RH degasser.

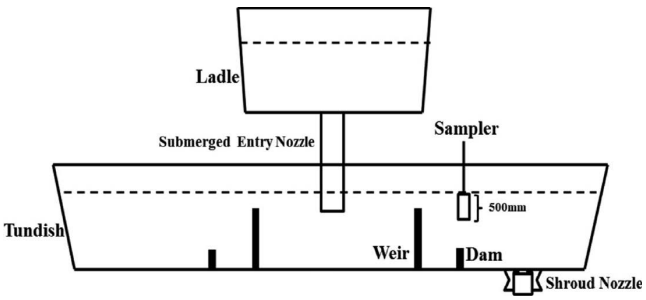

Fig. 2. Sampling position at Tundish.

Crystal Size Distribution (CSD) or PDF is a well-established subject in chemical engineering and geologic fields,[15–19] and the methodology adopted in the previous report by Zinngrebe *et al.*[7] is also applied to the present study. While the size distribution results can be variable depending on arbitrary observer's choices for bin size setting, PDF results will show a constant distribution regardless of bin size setting. A general description of PDF can be seen in Eq. (1) where the population density $n(v)$ of a certain size (l) is determined by an interesting bin size.

$$PDF = \frac{n_v(L_{xy})}{(L_y - L_x)} \quad \text{..... (1)}$$

The stereologically corrected PDF were calculated for all data sets using this method and plotted against the equivalent inclusion diameter. A detailed discussion on the procedure to calculate PDF can be found in previous studies.[12–14]

3. Results

3.1. Lognormal and Fractal Distribution

The size distribution of the inclusion population after deoxidization is the result of a combination of nucleation, growth and removal. Therefore, each size distribution can represent the evolution of the inclusion population. Lognormal and Fractal distributions were well known to be relevant to the fragmentation phenomena for mineral.[21] Those two distributions of PDF were successfully applied to the inclusion evolution by Ende[6,8] and Zinngrebe *et al.*[7]

Figure 3 represents a schematic of inclusion size distribution according to the time, measured after nucleation. Immediately after nucleation, the size distribution is parabolic, with a maximum number density at small inclusion size, as denoted graph ① in the Fig. 3. This distribution shows time-dependent and size-dependent growth, which is called Lognormal distribution. Lognormal distribution is defined by two parameters such as the Median, the Standard deviation. The formula for Lognormal distribution is described in Eq. (2).

$$f(x) = \frac{1}{x\delta_{\ln}\sqrt{2\pi}} \exp\left(-\frac{(\ln(x)) - \ln(m))^2}{2\delta_{\ln}^2}\right) \quad \text{..... (2)}$$

$f(x)$ is the PDF function of inclusions where $\delta_{\ln}$ is the Standard deviation which affects distribution shape and m is the Median which affects scale parameter.

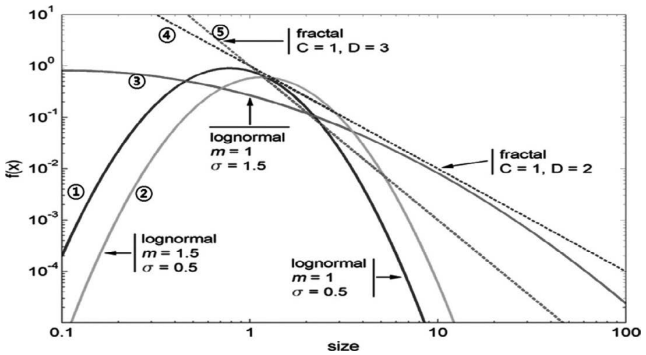

Fig. 3. Time evolution of representative size distributions of lognormal and fractal.

As time passes, the size distribution become broader and the position of the maximum number density is shifted to the right, and finally the shape of size distribution becomes linear as shown graph ⑤ in Fig. 3. This distribution show size-independent growth, which is called Fractal distribution. The formula for Fractal distribution is described in Eq. (3). This distribution is a straight line with a slope showing the scale invariance.

$$f(x) = C \cdot x^{-D} \quad \text{..... (3)}$$

Where the exponent D is the slope of the line and C is pre-factor constant setting the population level. The difference between Lognormal and Fractal distribution behavior can be explained by theories of nucleation, growth by diffusion and collision, removal by coalescence. Lognormal distribution indicates active nucleation which stands for active transfer of matter from solute to phase, while Fractal distribution indicates growth and removal which stands for no net mass transfer.[7]

3.2. PDF Behavior of Inclusions

Immediately after Al deoxidization, a large amount of nucleated inclusions will grow abruptly by diffusion and collision. **Figure 4** represents the inclusions observed from the sample taken at about 180 s after Al deoxidization, where the inclusions can be classified into two groups, clustered and insolated inclusion. In this study, we adopted a number density of 0.0025 μm^2 as the classification criterion for the inclusions, which is similar as Zinngrebe *et al.*[7] used. Therefore, the inclusions of which number density is larger than 0.0025 μm^2 (1ea in 20×20 μm) will be regarded as clustered. Indeed, the clustered and isolated inclusions show different behavior with each other. For clustered inclusions, there will be no opportunity to collide with isolated inclusions or other clustered inclusions of molten steel. Instead, only the inclusions which placed in outer part of cluster have chances to collide with others. Accordingly, the inner cluster inclusions will follow only Oswald ripening mechanism while isolated inclusions can be grown by both Oswald ripening and collision. It is worthy to note that the distribution of clustered inclusions shows lognormal distri-

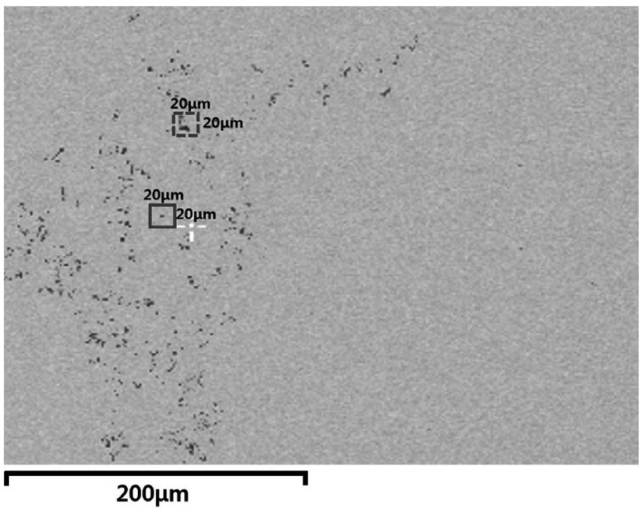

Fig. 4. Overview of inclusions at 180 s after Al deoxidization (broken line: clustered inclusions, solid line: isolated inclusions).

bution while the isolated inclusion reveals fractal distribution, which is consistent with the results of Zinngrebe *et al.*[7]

Because the larger inclusions can easily be eliminated during the RH process, the fractal distribution can be shown at the end of RH process when there is no further nucleation. In this study, overall 16 series of RH-Tundish-Slab samples have been analyzed. At finishing point of RH process, clustered inclusions were discovered at 5 different series among the all samples from 16 series. As those clustered inclusions turned out to be the results of turbulent floatation in the lollypop sampler, they have been excluded from the analysis results in **Fig. 5**. As can be seen in Fig. 5, all samples show fractal distribution of the PDF at the end of RH degassing process, which in accordance with Zinngrebe *et al.*[7]

3.3. PDF during Normal and Abnormal Operations

Figure 6 represents overall PDF results from the samples taken at RH and Tundish. During normal operation without considerable reoxidization, the fractal distribution can be observed at the samples from tundish, which are consistent with reference line taken from the samples at RH. This implies that there had not been the meaningful amount of newly nucleated inclusions in the samples. **Figures 7** and **8** show detailed PDF distributions during normal operation of continuous casting process when 150 ton and 50 ton of molten steel is left at ladle, respectively. Also, **Fig. 9** shows PDF results obtained at slab samples after normal operations.

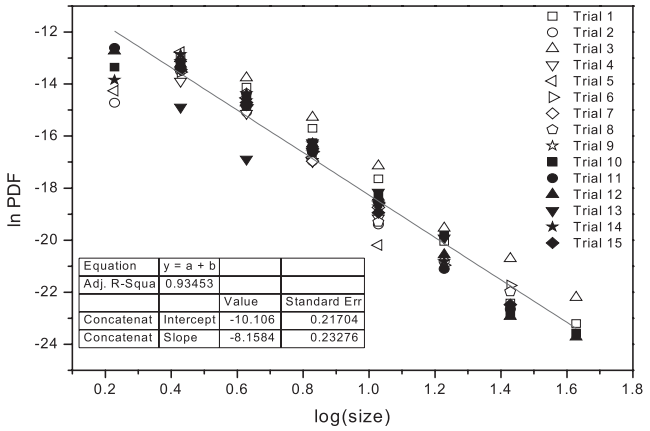

Fig. 5. Measured PDF for all samples at the end of RH degassing process.

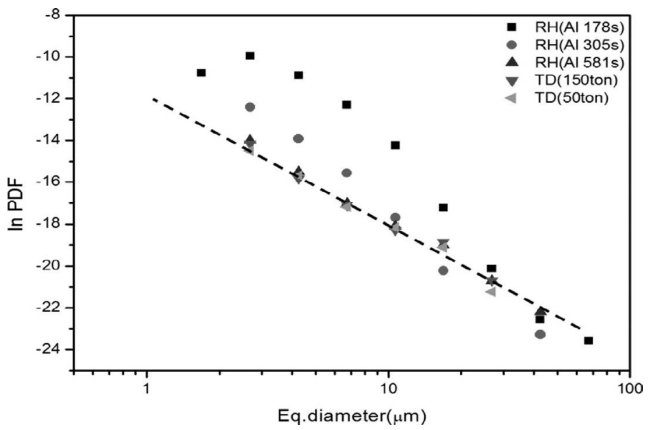

Fig. 6. Measured PDF during normal operations at tundish.

Figure 10 shows all PDF results of Figs. 6–9 and the PDF at RH finishing point reported by Zinngrebe *et al.*[7] for comparison. In this Figure, all PDFs show fractal distribution. Furthermore, the absolute vale of tangent line and y axis vale decreases according to the change of reactor. This implies that the change of exponent and y axis value is variable due to a continuous growth and removal of inclusions

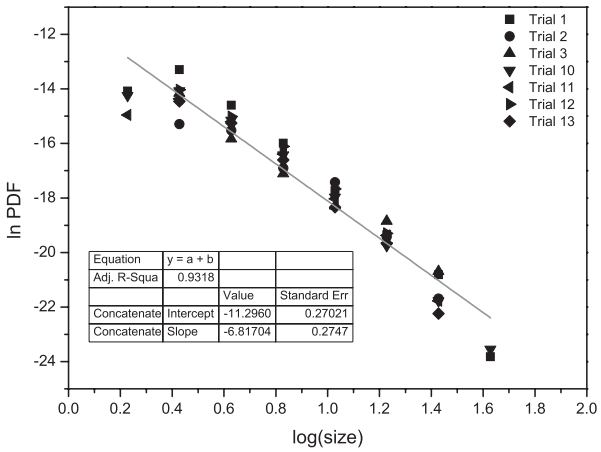

Fig. 7. Measured PDF during normal operation at tundish with 150 ton of molten steel.

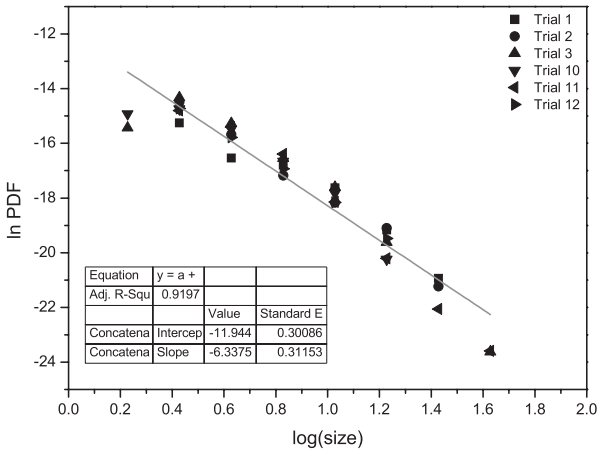

Fig. 8. Measured PDF during normal operation at tundish with 50 ton of molten steel.

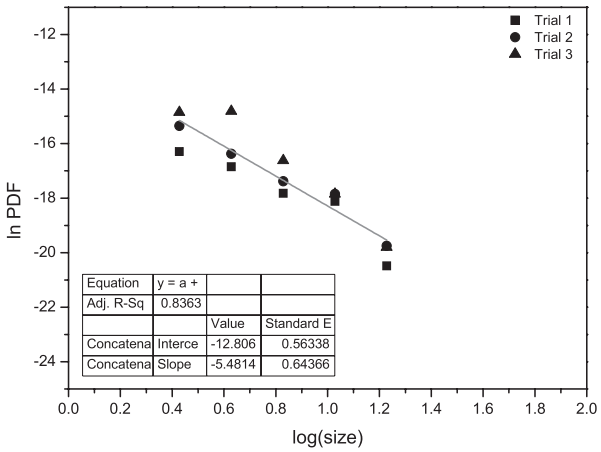

Fig. 9. Measured PDF during normal operation at a cast slab.

by collision and combination.

An example series of PDF can be seen in **Fig. 11**, where the abnormal reoxidization has been occurred during tundish operation. Fractal behavior can be observed at the finishing point of RH process regardless of the abnormal reoxidization at tundish. The PDF taken from TD and slab samples represents lognormal distribution which presumably caused by inclusions originated by reoxidization. It should be noted that the deviation compared to reference line is substantial for any abnormal samples.

4. Discussion

As mentioned previously the PDF distribution will not be affected by the bin. Therefore, it is desirable for any density function reported to be converted into the PDF distribution for comparison. For example, the density function from Zhang *et al.*[1] has been converted into PDF using Eq. (4), and shown in **Fig. 12**.

$$\log(PDF) = \log n(L_X, L_Y) - \log(L_Y - L_X) \quad \text{..... (4)}$$

It shows lognormal distribution at 1 s, 10 s and 30 s after deoxidization by Aluminum, and changes to fractal distribution at 120 s and 300 s after deoxidization by Aluminum.

On the contrary, it still shows lognormal distribution even at 305 seconds after deoxidization during commercial operation, as previously shown in Fig. 6. This arises from the addition of Ti alloy at 200 s after aluminum deoxidization during commercial operation. As can be seen in **Fig. 13**, Al_2O_3 inclusions react with Ti to form Al–Ti–O complex inclusions immediately after Ti addition due to the Al

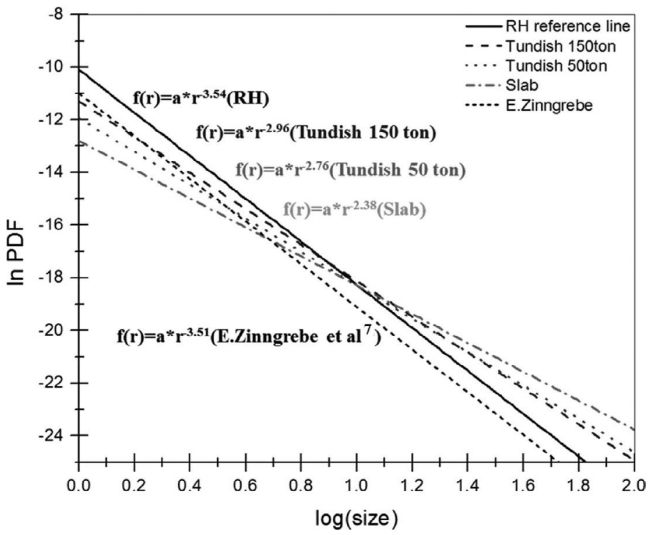

Fig. 10. Summary of measured PDF during normal operation at RH degasser, Tundish and Slab.

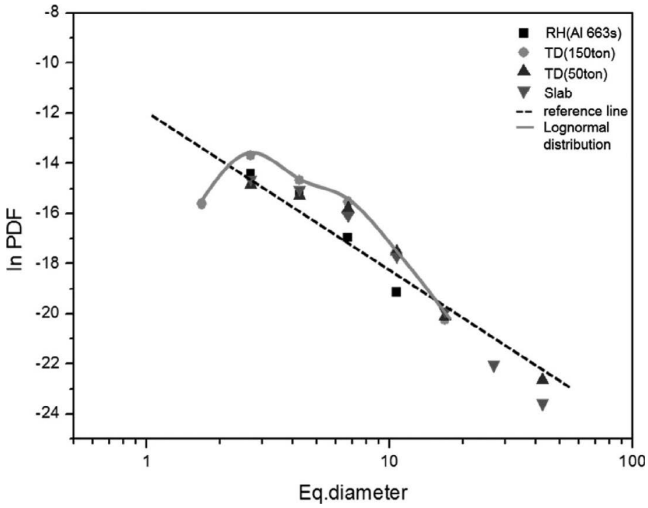

Fig. 11. Measured PDF during abnormal operation at Tundish.

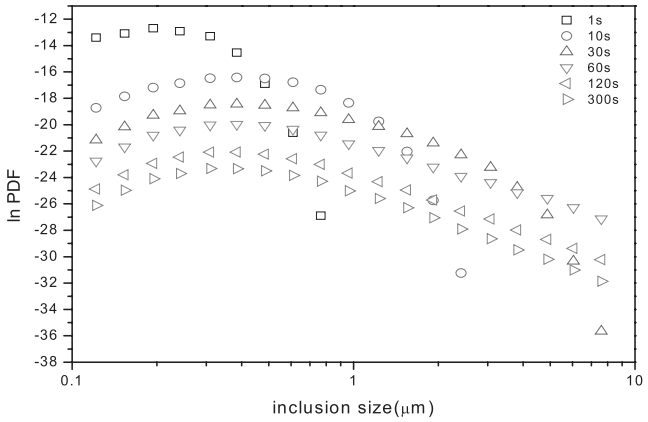

Fig. 12. Time evolution of size distribution based on PDF function versus size.

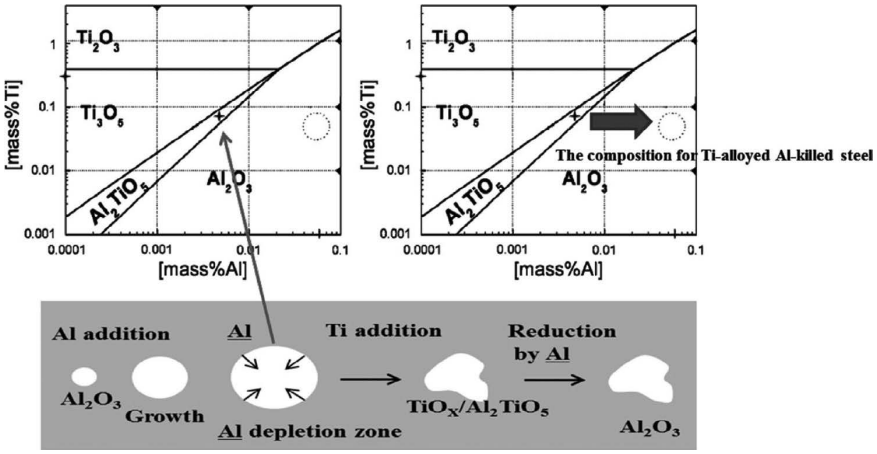

Fig. 13. Illustration of the inclusion change in Ti-alloyed Al killed steel.[22–24]

depleted zone in the vicinity of growing alumina.[22–24] Then, the complex inclusion will be reduced to pure alumina by diffused aluminum in matrix. Accordingly, it requires a certain amount of time to represent the fractal distribution after finishing the steps in Fig. 13.

As previously mentioned in Fig. 10, the slope of RH reference line from Zinngrebe *et al.*[7] and this research are very similar to each other, –3.52 and –3.55 respectively. The slopes of fractal distribution in Fig. 12 are also nearly the same, –3.55 at 120 s and –3.6 at 300 s respectively. Other researches[4,5] on alumina inclusion reveals analogous value of –3.3. Considering these results, a reference fractal distribution has been derived for alumina inclusions in ultra low carbon grade Al-killed steel as below.

$$f(x) = a \cdot x^{-3.55} \quad \text{..... (5)}$$

, where $f(x)$ is PDF of alumina inclusion, x is diameter of inclusion, a is a constant which represents the degree of initial deoxidization.

The slope of any PDF distributions can be considered as saturation value of alumina inclusions' coalescence phenomenon which is relevant to interface energy of alumina inclusion. Therefore, Eq. (5) in this study would be extremely useful to evaluate the efficiency of any steelmaking process. For example, it can be used to confirm the point of nucleus formation by unexpected reoxidization, and to determine the optimum processing time when the PDF of inclusions reaches the reference distribution.

Figure 14 represents the composition change of Al and N in molten steel during RH and Tundish operations. Generally, the change of Al or N concentration has been considered to be a measure of reoxidization during steelmaking and casting operations. Therefore, it should be meaningful to make comparison of compositional change of Al or N with the PDF distribution. In case of the normal operations when the PDF shows a negligible deviation from the fractal reference, the compositional changes also were insignificant for both Al and N as can be seen in Fig. 14, where Al loss were 23 ppm and 51 ppm respectively, and N loss could not be found at all. On the contrary, relatively larger amount of Al or N low have been observed for abnormal operations when the PDF deviated considerably from the fractal reference; 116 ppm and 102 ppm of Al loss, 2 ppm and 1 ppm of N loss, respectively. Therefore, it can be concluded that the chemical composition changes were consistent with PDF analysis in this study.

Table 1 summarizes comprehensively the results of alumina inclusion size distributions by Zinngrebe *et al.*[7] and Zhang *et al.*[1] and this research. As can be seen in Table 1, the inclusion size distribution shows fractal distribution after a certain amount of time in all three research results. Also, the exponents of PDF are almost the same as –3.55 at the end of secondary refining process in a ladle. However, it should be noted that there were meaningful change of fractal distribution according to the reactor, which could not be found in any previous reports. As can be seen in Fig. 10, the slope of the graphs which are equivalent to the exponents in fractal distribution increases with the progress of the process such as –2.76 at TD 50 ton and –2.38 at slab. This behavior is believed to be caused by either reoxidization at Tundish and/or mold or different fluid conditions at each metallurgical reactor which eventually generates variations in fractal distribution slope. The inclusion size distribution controlled by physical coalescence or breakup of inclusion must be dependent not only on the physical properties of the inclusion such as interface energy of inclusion, but also the possibility of coalescence which can be affected by the flow of molten steel. Accordingly, it is highly conclusive that the changes in fluid condition will bring considerable variations on fractal reference distribution.

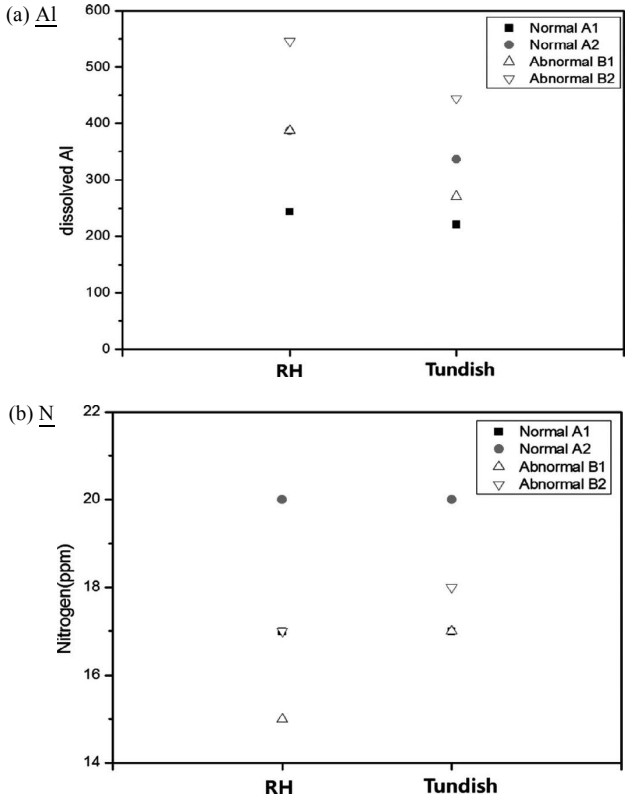

Fig. 14. Compositional evolution of the steel between RH degassing and Tundish.

Table 1. Comparison of evolution of inclusion size distribution.

	Zinngrebe[7]	J. Zhang[1]	present study
Method	Sampling analysis	simulation	Sampling analysis
Reactor	RH→Tundish→ StirringStation→Mold	ladle	RH→Tundish →Slab
Size distribution	Fractal	Fractal	Fractal
Gradient value	–3.51	–3.60	–3.55
Gradient change	No	–3.16 (60 s)	–3.55 (RH)
		–3.55 (120 s)	–2.76 (TD 50 ton)
		–3.60 (300 s)	–2.38 (Slab)
PDF value change	Furture investrigated.	Reduce	Reduce (<1 um)
		(Saturation)	Increase (>1 um)

5. Conclusion

In the present study, Ti-alloyed Al-killed steels were analyzed to clarify evolution of alumina inclusions during steelmaking and cast process after Al deoxidization. In order to quantify inclusion density function, automated inclusion

analysis (AIA) SEM technique is applied. Three dimensional PDF is obtained by using CSD Correction program. Inclusion PDF according to the size of inclusion shows either lognormal distribution or fractal distribution. From the inclusion PDF distributions, the major findings are as follows:

(1) During RH operations, the lognormal distribution was revealed after 180 s of Al addition. Also, the fractal distribution was obtained after 400–600 s of Al addition. The delayed appearance of fractal distribution arises from the formation of complex inclusion, Al–Ti–O, after Ti addition.

(2) The fractal distribution at the end of RH operation could be expressed as an equation, $F(x) = a \cdot x^{-3.55}$, where $F(x)$ is PDF of inclusions, x is diameter of inclusions and a is a constant relevant to the degree of initial deoxidization and fluid dynamics. This equation can be used for evaluation of the degree of reoxidization during steelmaking process.

(3) After RH process, the exponents of fractal distribution were changed to be –2.76 in tundish and –2.38 in slabs, respectively. This implies that the fractal distribution will vary with different reactors or reservoirs of molten steel.

(4) During any abnormal operations, the deviation of PDF from the reference distribution is in accordance with compositional change of molten steel such as the increase of nitrogen pick-up and the decrease of soluble aluminum.

Acknowledgements

Financial support from POSCO is gratefully acknowledged. The authors want to express their gratitude for the helpful discussions and technical support to Mr. Y. H Jhang in POSCO and Mr. J. K Lee in RIST. Also, the authors thank Professor M. Higgins in Quebec University for in-depth discussions and kind suggestions regarding the application of CSD Correction program.

REFERENCES

1) J. Zhang and H.-G. Lee: *ISIJ Int.*, **44** (2004), 1629.
2) U. Lindborg and K. Torssell: *Trans. Metall. Soc. AIME*, **242** (1968), 94.
3) A. K. Sinha and Y. Sahai: *ISIJ Int.*, **33** (1993), 556.
4) Y.-J. Kwon and H.-G. Lee: *ISIJ Int.*, **48** (2008), 891.
5) L. Zhang and W. Plushkell: *Ironmaking Steelmaking*, **30** (2003), 106.
6) M. A.Van Ende, M. Guo and E. Zinngrebe: *Ironmaking Steelmaking*, **36** (2009), 201.
7) E. Zinngrebe, C. Van Hoek and I.-H. Jung: *ISIJ Int.*, **52** (2012), 52.
8) M. A. Van Ende: PhD Thesis, KU LEUVEN, (2009).
9) H. Suito and H. Ohta: *ISIJ Int.*, **46** (2006), 33.
10) H. Ohta and H. Suito: *ISIJ Int.*, **46** (2006), 14.
11) M. Wakoh and N. Sano: *ISIJ Int.*, **47** (2007), 627.
12) A. K. and H. Suito: *Metall. Mater. Trans. B*, **30** (1999), 259.
13) Y. Miki and B. G. Thomas: *Metall. Mater. Trans. B*, **30** (1999), 639.
14) A. D. Randolph and M. A. Larson: Theory of Particle Processes, Academic Press, New York, (1971).
15) B. D. Marsh: *Contrib. Mineral. Petr.*, **99** (1988), 277.
16) M. Higgins: *J. Petrology*, **39** (1998), 1307.
17) M. Higgins: *Amer. Mineralogist*, **85** (2000), 1105.
18) M. Higgins: *Amer. Mineralogist*, **87** (2002), 171.
19) B. D. Marsh: *J. Petrology*, **39** (1998), 553.
20) http://wwwdsa.uqac.ca/~mhiggins/csdcorrections.html
21) I. N. Bindeman: *Amer. Mineralogist*, **90** (2005), 1801.
22) C. Wang, N. T. Nufher and S. Sridhar: *Metall. Mater. Trans. B*, **41** (2010), 1094.
23) C. Wang, N. T. Nufher and S. Sridhar: *Metall. Mater. Trans. B*, **40** (2009), 1021.
24) C. Wang, N. T. Nufher and S. Sridhar: *Metall. Mater. Trans. B*, **40** (2009), 1034.